ELSEVIER

Journal of Alloys and Compounds 446–447 (2007) 336–341

Journal of ALLOYS AND COMPOUNDS

www.elsevier.com/locate/jallcom

Li–Mg–N–H: Recent investigations and development

Weifang Luo [a,*], Jim Wang [a], Ken Stewart [a], Miles Clift [a], Karl Gross [b]

[a] *Sandia National Laboratories, 7011 East Eve., Livermore, CA 94550, USA*
[b] *HyEnergy LLC, Newark, CA, USA*

Received 30 September 2006; received in revised form 10 November 2006; accepted 13 November 2006
Available online 5 December 2006

Abstract

Metal amide containing material is one of the more promising hydrogen storage materials for motor vehicular "on-board" applications. One of the issues related to the application of metal–N–H storage systems is NH_3-formation that takes place simultaneously with H_2 release. NH_3 in desorbed hydrogen, when feeding a fuel cell, will not only damage the catalyst in the fuel cell, but also accelerate the material degradation. Accurate determination of the amounts of NH_3 in the H_2 is, therefore, very important. A novel method to quantify NH_3 in the desorbed H_2, the Draeger Tube, is reported to be suitable for this purpose. The results indicate that the concentration of NH_3 in the desorbed H_2 from the ($2LiNH_2 + MgH_2$) system increases with desorption temperatures, from 180 ppm at 180 °C to 720 ppm at 240 °C. The capacity loss after 270 cycles at a temperature of 200 °C is 25%, with 1/3 of the loss due to NH_3-formation. More research is needed to determine the cause for the remaining capacity loss. This cyclic stability is very encouraging for a material prior to any formulation optimization. A water-saturated air exposure of the desorbed sample at 220 °C for 21 h, after a sequence of air-exposures at lower temperatures, was found to not affect its capacity or kinetics in subsequent desorption runs.

Keywords: Hydrogen storage; Metal-amide–hydride; Thermodynamics; Ammonia; Cyclic stability

1. Introduction

Chen et al. [1] initially proposed lithium nitride/imide as a hydrogen storage material due to its high hydrogen capacity, up to 11.5 wt.%. The decomposition of ($LiNH_2 + 2LiH$) is a two-step reaction [1] as shown below:

$$LiNH_2 + 2LiH \Leftrightarrow Li_2NH + LiH + H_2 \Leftrightarrow Li_3N + 2H_2 \quad (1)$$

Following Chen's article a large number of papers have been published [2–14] on amide/hydride systems. We reported a significant improvement of the storage features of the Li–N–H system by partial substitution of Mg for Li, which delivered H_2 at 30 bar (200 °C) with a reversible capacity of 5.2 wt.% or more with fast kinetics [7,13]. Chen et al. further reported the effect of substitution of various elements on the stability of the Li–N–H system [5,8]. Ichikawa et al. reported sorption reversibility and kinetics of the $LiNH_2 + LiH$ system [2] and isotherms for the $3Mg(NH_2)_2$–8LiH system [3]. Nakamori et al. [4,6] reported the effect of Mg substitution on the stability of the Li imide/amide systems. Chen et al. proposed a destabilization mechanism for the amide–hydride system [5,10] and Luo et al. proposed a reaction mechanism for the ($2LiNH_2$–MgH_2) system [13,14].

For the ($2LiNH_2 + MgH_2$) system, there is a crystal structure conversion/chemical reaction process that takes place at 220 °C under a hydrogen pressure of 100 bar (10 MPa) [14] before any sorption reaction occurs:

$$2LiNH_2 + MgH_2 \Rightarrow Mg(NH_2)_2 + 2LiH. \quad (2)$$

The subsequent reversible hydrogen release/uptake reaction is:

$$Mg(NH_2)_2 + 2LiH \Leftrightarrow Li_2Mg(NH)_2 + 2H_2. \quad (3)$$

There is also a possible reaction, $Mg(NH_2)_2$ self-decomposition, which can take place parallel with reaction (3):

$$3Mg(NH_2)_2 \Rightarrow 3MgNH + 3NH_3 \Rightarrow Mg_3N_2 + 4NH_3. \quad (4)$$

If reactions (3) and (4) occur, H_2 and NH_3 should be present simultaneously in the desorbed gas [15]. The ratio of H_2 and

* Corresponding author. Tel.: +1 925 294 3729; fax: +1 925 294 3410.
E-mail address: wluo@sandia.gov (W. Luo).

0925-8388/$ – see front matter © 2006 Elsevier B.V. All rights reserved.
doi:10.1016/j.jallcom.2006.11.067

NH_3 concentrations in the desorbed gas depends on the relative rates of reactions (3) and (4). NH_3 concentration determination is very important since NH_3 in desorbed H_2, when feeding a fuel cell, will deactivate the Pt catalysts in a fuel cell and, moreover, NH_3 formation also reduces the material storage capacity.

Previous attempts to obtain consistent values of the NH_3 concentrations in the desorbed H_2 by using a residual gas analyzer (RGA), infra-red (IR) and gas chromatography (GC) were unsuccessful because of the strong adsorption of NH_3 on the inner wall surfaces of these instruments before the gas sample reached the instruments' detectors. In this study, we report the results obtained by using a novel method, the Draeger Tube [16], to quantify the NH_3 concentrations in the desorbed H_2. The Draeger Tube^{TM} is a commercially available product, which has been used in the petroleum refinery industry for decades to detect the impurity, NH_3, concentrations in a mixture of hydrocarbon compounds before feeding the refinery reactor, which contains a Pt catalyst. The tolerance of Pt towards NH_3 has not been well defined; <1 ppm is probably a reasonable value. The resolution and accuracy of this method is proved to be able to satisfy the purpose of quantitatively determining the NH_3 concentration in the desorbed H_2.

In addition, the cyclic stability and the sensitivity of the storage material towards air exposure are also very important features for applications. These will be reported and discussed here.

2. Experimental details

2.1. Source materials and sorption measurement method

The starting materials, lithium amide ($LiNH_2$) (Purity 95% from Aldrich) and magnesium hydride (MgH_2) (Purity 95% from Pfaltz & Bauer) were used without pre-treatment.

A fresh sample was a mixture of $LiNH_2$ and MgH_2 in a molar ratio of 2:1.1. A mixture of $LiNH_2$ and MgH_2 was mechanically milled in the glove box under an argon atmosphere using a Fritsch mill with 40 WC milling balls each weighing 8 g. The sample sizes and milling conditions in the NH_3 analyses, cycle life and water-saturated-air exposure are slightly different and they will be described in the following sections separately.

The Sieverts'-type system for the sorption process measurement have been described elsewhere [7,13,14].

2.2. Powder XRD measurements

Powder X-ray diffraction (XRD) patterns were collected on a SCINTAG (XDS 2000) powder diffractometer at step increments of 0.05° measured during 0.5 s ($\lambda = 1.5406$ Å). During scanning, the samples were protected from oxidation by a thin Mylar sheet wrapping. Data were collected for the desorbed samples after three cycles, 270 cycles and air-exposure, separately.

2.3. Analysis of NH_3 in H_2

The sample used for this test was 1.5 g, from a large size mill of 30 g. The milling conditions were 5 repetitions at 300 rpm (30 min milling interspersed with periods of rest time of 90 min) then 12 repetitions at 350 rpm (30 min milling interspersed with periods of rest time of 90 min) followed by 50 repetitions at 350 rpm (30 min milling interspersed with a periods of rest time of 150 min). The purpose of alternating the milling with rest times is to keep the sample from being overheated by the milling.

The milled sample was subjected to 5-absorption/desorption cycles at 220 °C before NH_3 analysis to ensure that the sample had its desired sorption properties.

NH_3 formation was monitored by measuring its concentrations in the desorbed H_2 using a Draeger Tube [16]. The amount of a gas sample, which passed through the Draeger tube, was 100 ml at room temperature and 1 atm of pressure. Larger sample sizes may be needed when the NH_3 concentration is small according to the instructions provided by the Draeger Tube manufacturer. The color of a Draeger Tube changes from yellow to dark blue after NH_3 passes through and the length of the portion with color change is proportional to the concentration of NH_3 in the gas. The NH_3 concentration can, therefore, be read from the scores on the body of the Tube, as shown in Fig. 1(a).

The following procedures were used when apply Draeger Tube to the measurement of the NH_3 concentration in desorbed hydrogen:

(1) The sample was fully absorbed at H_2–pressure of 100 bar and 220 °C.
(2) The sample was cooled to room temperature, then H_2 pressure was released further evacuated at room temperature to ensure that the gas being sent to the Tube for NH_3 concentration measurement was released from the sample only and not the residual gas from the previous absorption.
(3) The sample temperature was then raised to the designed values and the gas collected in a dosing volume of an appropriate size to ensure the gas pressure to be slightly above 1 atm.
(4) The sample holder was connected to the special gas hand-pump, provided by the Tube manufacturer, with a Draeger Tube as shown in Fig. 1(b). The desorbed hydrogen sample flow rate, recommended by the Tube manufacturer, was carefully controlled by the valve attached to the sample holder. The flow stopped when 100 ml of gaseous sample was collected by the hand pump.
(5) The NH_3 concentration readings were read from the scores on the Tube.

2.4. Cycle life test

The sample used for this test was 3 g, from a small size mill of 6 g. The milling conditions were 30 repetitions at 300 rpm (30 min milling interspersed with periods of rest time of 90 min). The purpose of alternating the milling with rest times is to keep the sample from being overheated by the milling.

The milled sample was subjected to a soaking period at H_2-pressure of 100 bar (10 MPa) and a temperature of 220 °C for 6 days, followed by 10-absorption/desorption cycles at 200 and 220 °C before NH_3 analysis to ensure the quality of the sample.

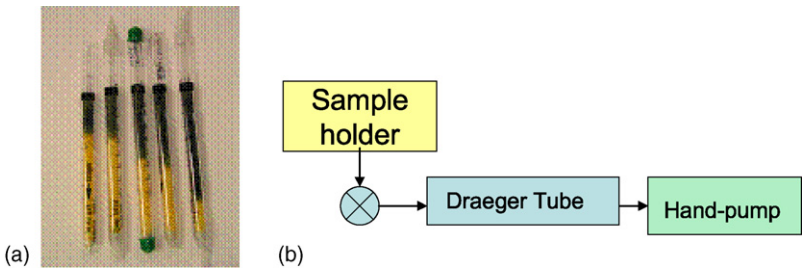

Fig. 1. (a) Draeger Tubes after NH_3-containing gases, at various concentrations, passing through; (b) Schematic flow-chart for sending desorbed hydrogen to Draeger Tube for NH_3 concentration determination.

The cycle life test was then carried out at 200 °C and at a constant hydrogen pressure of 110 bar (11 MPa). The durations of absorption/desorption were controlled by a timer built in a Lab View based program used for data acquisition. The amount of H_2 desorbed was measured by a Sieverts'-type system with an initial reservoir pressure of zero and at 0.5 bar (0.05 MPa) at the end of each desorption cycle. Data were recorded for the desorption runs, not for absorption, in order to minimize the size of the data file.

2.5. Water saturated-air exposure measurement

The sample for this test was 1.5 g, from a mill of 10 g. The milling conditions were 42 repetitions at 300 rpm (30 min milling interspersed with periods of rest time of 150 min).

The milled sample was subjected to a soaking period at a H_2-pressure of 100 bar (10 MPa) and a temperature of 220 °C for 6 days and followed by 10-absorption/desorption cycles at 200–220 °C before air-exposure measurement to ensure the quality of the sample and to obtain the desorption profiles needed for comparison with those after the air-exposure.

In this study the air exposure was applied only to the desorbed sample. After a desorption run the sample was evacuated at 220 °C for 30 min, it was then cooled down to the next planned exposure temperature. In this experiment, atmospheric air was bubbled through water. The air was then allowed to enter the sample chamber at the designed temperatures for a given time period. The air was confirmed to be water-saturated by forming a water condensation layer on a mirror. At the end of the air exposure, the temperature of the sample was increased to 220 °C, evacuated to remove the residual air and then the sample was re-hydrogenated at 220 °C.

In this study the comparisons of the profiles of desorption at 220 °C before and after the H_2O-saturated-air exposures were used to evaluate the effect of H_2O-saturated-air exposure on the performance of the material.

3. Results and discussions

3.1. NH_3-formation

Three certified H_2 gas samples, with NH_3 concentrations of 103, 502 and 1035 ppm, were used to crosscheck the accuracy of the Draeger tubes before they were applied for measurement of the NH_3 concentrations. Fig. 2 shows the values of the NH_3 concentrations in the certified hydrogen (the rated values) versus those read out from the Draeger tubes after the certified gases had passed through (the measured values). It can be seen that the measured values agree with the rated values of the certified gases very well.

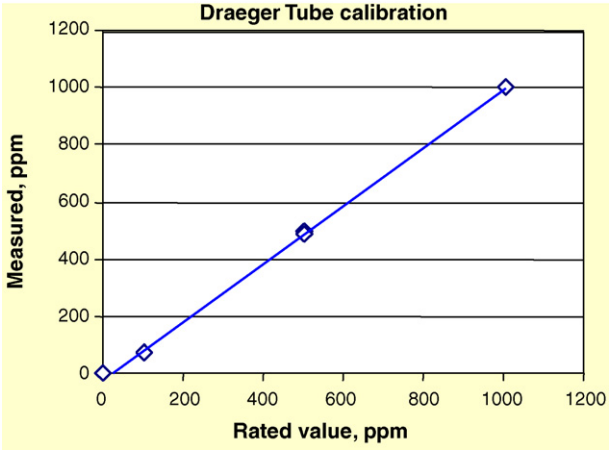

Fig. 2. The crosscheck results for Draeger Tube (the measured) using certified gases of hydrogen with NH_3 concentrations of 103, 502 and 1031 ppm (the rated values).

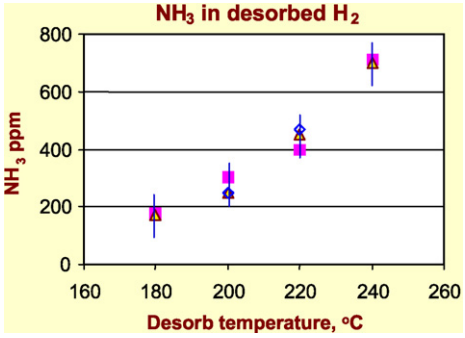

Fig. 3. NH_3 concentrations in H_2 desorbed as a function of desorption temperatures measured by Draeger Tube. There are 2–3 data points, indicated by different symbols, for each temperature.

A Draeger Tube was then applied to the measurement of the NH_3 concentration in the desorbed H_2. Fig. 3 shows the dependence of NH_3 concentration on the desorption temperature. It can be seen that the higher is the desorption-temperature, the greater is the NH_3 concentration. The measured NH_3 concentrations were 180 ppm at 180 °C and 720 ppm at 240 °C.

As mentioned above, reactions (3) and (4) in the system of $(Mg(NH_2)_2 + 2LiH)$, can occur simultaneously. Fig. 4 shows the differential scanning calorimeter (DSC) results [10] at various scan rates for these two reactions. The group of profiles on the left side corresponds to the reaction (3) and the one on the right side corresponds to reaction (4). At a desorption temperature of 200 °C for reaction (3), the hydrogen release reaction, peaked, while the NH_3 release reaction rate (reaction (4)) was still very low. This is the reason why only low levels of NH_3 were detected in the measurements (Fig. 3). It is apparent from Fig. 4 that NH_3 concentration increases with desorption temperature. More well cycled samples are needed to confirm the existance of the peak at 21.4°.

The self-decomposition of amide, reaction (4), degrades the H-storage capacity of the Li–Mg–N–H system since, after loosing nitrogen through NH_3-formation, the system becomes

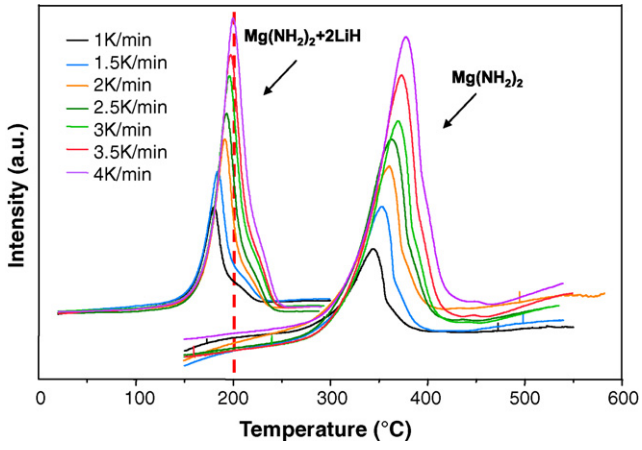

Fig. 4. DSC profiles for $(Mg(NH_2)_2 + 2LiH)$ and $Mg(NH_2)_2$ at various scan rates [10].

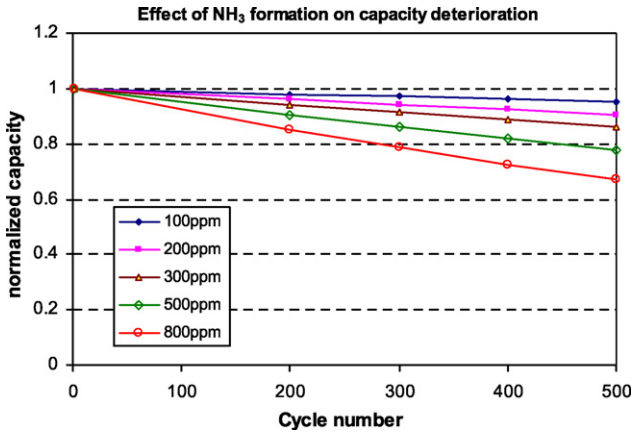

Fig. 5. Calculated capacity degradation resulting from NH_3 formation during desorption at concentrations from 100 to 800 ppm.

Li–Mg–H, which does not function properly as a storage system at a temperature of ~200 °C.

The degradation of the capacity due to NH_3-formation can be estimated from the concentration of NH_3 in the desorbed H_2. For example, assuming the NH_3 concentration in desorbed H_2 to be A (in ppm), the relationship of $C_{n+1} = C_n\ (1 - A \times 10^{-6})$ holds where C_n and C_{n+1} are the capacities of the nth and the $(n+1)$th cycles, respectively. A more general equation can be derived for the capacity of the nth cycle assuming a constant NH_3 concentration (A, ppm) in the desorbed H_2, i.e.,

$$C_n = C_1(1 - A \times 10^{-6})^n, \quad (5)$$

where C_1 is the capacity for the first cycle. Fig. 5 has been constructed according to Eq. (5) for NH_3 concentrations between 100 and 800 ppm. It can be seen that after 500 cycles the capacity reduction should be 5 and 32% for NH_3 concentrations of 100 and 800 ppm, respectively.

It is important to control the NH_3-formation in order to improve the cyclic stability of this material. Ichikawa et al. reported an approach for lowering the NH_3 concentration in the desorbed H_2 by adding an excess amount of LiH to the Li–N–H system [2]. More effort is needed in future research to reduce NH_3-formation.

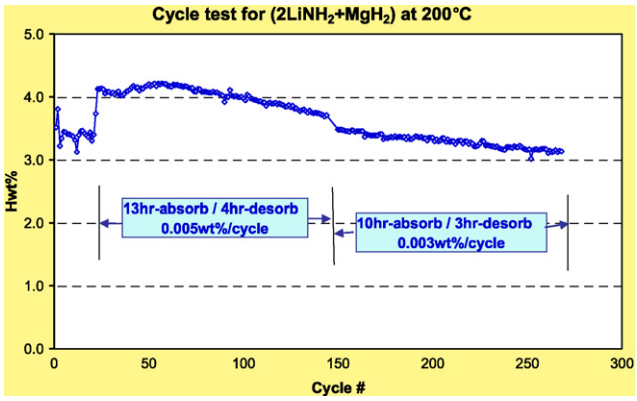

Fig. 7. $(2LiNH_2 + MgH_2)$ cycle test at 200 °C. The duration of sorption cycles and capacity loss for each cycle are marked.

3.2. Cyclic stability

The capacity values reported in the cycle life test strongly depend on the absorption/desorption conditions, such as the sorption temperatures, the initial and final pressures for each cycle, the durations for each sorption run, etc. Fig. 6 shows absorption (a) and desorption (b) profiles for this material. It can be seen that the desorption rate at 220 °C was much higher than that at 200 °C, i.e., 90% of desorption can be completed within half an hour at 220 °C while it required more than 2 h at 200 °C. For absorption, the rate at 220 °C was also much higher than that at 200 °C. At 200 °C, after 5 h, the absorption was far from completion since the absorption rate becomes slow when Hwt.% H > 1.2.

Fig. 7 shows the desorption capacities for 270 cycles. The duration for each cycle was changed after 144 cycles from 13 h-absorption/4 h-desorption cycles to 10 h-absorption/3 h-desorption for the remaining cycles. The capacities for the first 20 cycles were not fully utilized because the temperature and the sorption duration for each cycle were incorrectly set. After the 20th cycle, the capacity values reached the apparent maximum, 4.2 wt.%, which is below the expected value of 5 wt.%. The decreased capacity at 144th cycle resulted from the shortening of absorption/desorption times. It is also noticed that the

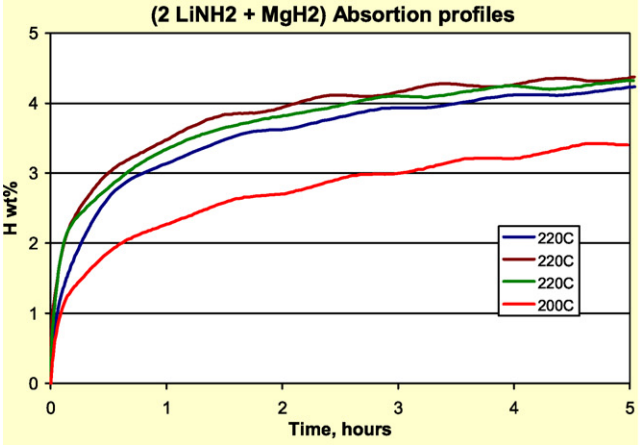

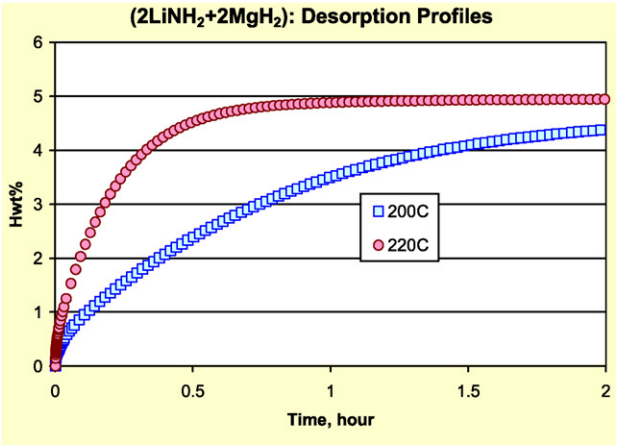

Fig. 6. $(2LiNH_2 + MgH_2)$ absorption(a)/desorption(b) profiles at 200 and 220 °C.

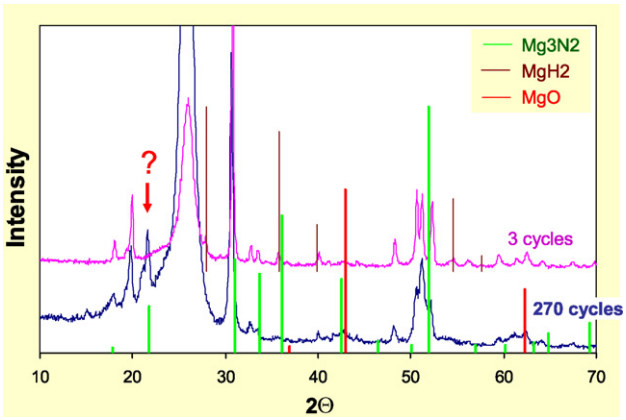

Fig. 8. Powder XRD patterns for the desorbed samples after 3 and 270 absorption/desorption cycles. The large peak at around 26.5° is resulting from the Mylar, the layer to protect the samples from oxidation.

capacity decrease is slower for cycles after the 144th cycle for an unknown reason. After 270 cycles, the total capacity reduction was 25%, compared with the peak capacity.

As mentioned above, the NH_3-formation accounts for a partial capacity loss during cycling. According to the calculated capacity loss due to the NH_3-formation (Eq. (5) and Fig. 5) using the NH_3 concentration value measured at 200 °C, 220 ppm (Fig. 3), the capacity loss after 270 cycles should be only about 7%, in other words, the majority of the capacity loss observed results from sources other than NH_3-formation. These could be, for example, incomplete absorption/desorption due to insufficient sorption times as mentioned above.

Fig. 8 shows the comparison of the powder XRD pattern for the sample after 270 absorption/desorption cycles, with the one after 3 cycles for comparison. It can be seen that most of the diffraction angles are identical for these two samples with only small variation of intensities. The diffraction angle of 21.4° of the sample with 270 cycles was the only new peak, although more well cycled samples are needed to confirm the existance of the peak at 21.4°. Among all hydrides, imides and nitrides that could possibly appear in this system, such as LiH, MgH_2, Li_2NH, MgNH, Li_3N and LiMgN, there was only one, Mg_3N_2, which has a diffration peak at this angle. The diffraction pattern of Mg_3N_2 was included in Fig. 8, however, the existance of the peak at 21.4° is insufficient evidence to support the presence of Mg_3N_2. The material with the peak at 21.4° remains unknown and more investigation is needed to identify this material and to understand the mechanism of the capacity reduction as well.

3.3. Effect of H_2O-saturated-air exposure on sorption performance

The H_2O-saturated-air exposure test is an extension of the work done by Luo et al. [17]. In the present study, a sequence of water-saturated-air exposures for much longer exposure time periods than before [17] were applied to the sample as shown in Table 1. The desorption profiles before (D1–D8) and after (D9–D20) the exposures are shown in Fig. 9. It can be seen that there is a small improvement, or at least no degradations, of the capacity or kinetics of desorption after these H_2O-saturated-air exposures.

Table 1
H_2O-saturated-air exposure

Cycle # before air exposure	Temperature (°C)	Exposure time (h)
9	22	0.33
11	25	2
14	53	16.5
16	96	16
18	180	18
20	220	21

Hu et al. reported the ultra fast desorption of a mixture of $LiNH_2$ with partially oxidized Li_3N [18,19]. They concluded that the Li_2O was acting like a catalyst for the sorption process for Li–N–H system. No similar powder XRD analysis has been reported in the literature for the air-exposed ($2LiNH_2 + MgH_2$).

The air-exposed desorbed sample after the 20th cycle was examined by powder XRD and the results were shown in Fig. 10. It can be seen that Li_2O is present both before and after air-exposure without any significant intensity differences. It can be seen that all the peaks are broadened after air-exposure. This indicates the existence of crystalline structural deformation in the air-exposure process. More prominently, the characteristic triple peaks for $Li_2Mg(NH)_2$ [14] between 50° and 53.4° became broadened and lost their individual identities, which may result from a significant deformation.

The presence of diffraction peaks at 43.15° and 62.5° indicates the presence MgO. The MgO formation may partially result from the oxidation of MgH_2 since there is a small amount of MgH_2 present in the sample before air-exposure, but not the one after air-exposure (Fig. 10). However, the amount of MgO formed seems to be much more than that would be result from

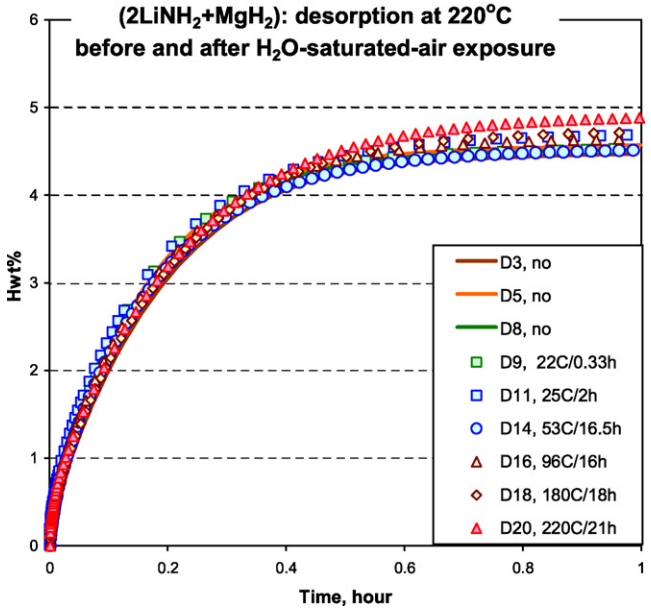

Fig. 9. Desorption profiles before and after H_2O-saturated air exposure.

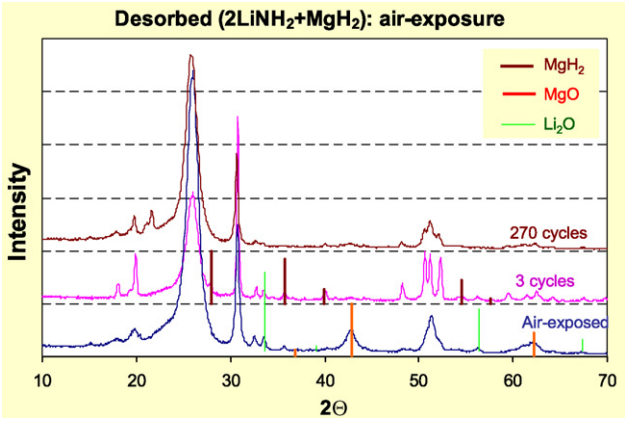

Fig. 10. Powder XRD profiles for samples before and after air-exposure. The profile after 270 cycles is included for comparison.

MgH_2 oxidation. The amount of MgO in air-exposed sample is much higher than the one after 270 cycles, as shown in Fig. 10.

In the air-exposed sample the presence of MgO, instead of Li_2O, was unexpected since the formation enthalpy of Li_2O is more exothermic than that for MgO. The formation of MgO may result from the existence of the Li–N bond, which reduces the activity of Li towards oxidation.

Hjort et al. [20] reported that hydrogen uptake rate by Mg increased with a thin layer of Mg oxide on the surface, although hydrogen uptake rate monotonically declined when the Mg oxide layer became thicker. They suggested that the increase of hydrogen uptake rate resulted from the Mg oxide nuclei, which served as nucleation centers for hydride growth. More work is needed to understand the mechanism of the effect of material oxidation of the Li–Mg–N–H system on its performance.

4. Conclusions

NH_3 formation results from amide self-decomposition which is a parallel competing process with H_2 release during the desorption process of the Li–Mg–N–H system. The Draeger Tube test is a very reliable method to determine the NH_3 concentration in the desorbed H_2. For the Li–Mg–N–H system, the temperature needed to form appreciable amounts of NH_3 is much higher than that for hydrogen release and, therefore, NH_3 concentrations are below 1000 ppm when desorption temperatures are below 240 °C. NH_3 concentration increases with the desorption temperature, from 180 ppm at 180 °C to 720 ppm at 240 °C.

270 sorption cycles have been completed for ($2LiNH_2 + MgH_2$) after which a 25% capacity reduction was observed. NH_3-formation can account for 7% of the capacity loss. The cause of the remaining capacity loss is unclear, although incomplete absorption/desorption may contribute to this loss. A new diffraction peak at 21.4° was observed in the powder XRD pattern of the desorbed sample after 270 cycles and its identity needs to be determined.

The capacity and kinetics of ($2LiNH_2 + MgH_2$) do not change after the desorbed sample was exposed to water-saturated air at 220 °C for 21 h, although the MgO is confirmed to be present in the air-exposed sample. More work is needed to understand the effect of material oxidation on the hydrogen uptake/release rates.

Acknowledgements

The authors thank Prof. T. B. Flanagan and S. Luo of Univ. Vermont for their original work on H_2O-saturated-air exposure experiments and valuable advice.

The authors thank Dr. Guang Zhang of Chevron Products Company for her recommendation to use Traeger Tube for NH_3 concentration determinations.

Sandia is a multi-program laboratory operated by Sandia Corporation, a Lockheed Martin Company, for the United States Department of Energy's National Nuclear Security Administration under contract DE-AC04-94AL85000.

References

[1] P. Chen, Z. Xiong, J. Luo, J. Lin, K.L. Tan, Nature 420 (2002) 302–304.
[2] T. Ichikawa, S. Isobe, N. Hanada, H. Fujii, J. Alloys Compd. 365 (2004) 271–276.
[3] T. Ichikawa, K. Tokoyoda, H. Leng, H. Fujii, J. Alloys Compd. 400 (2005) 245–248.
[4] Y. Nakamori, S. Orimo, Mater. Sci. Eng. B 108 (2003) 48–50.
[5] P. Chen, Z. Xiong, J. Luo, K. Tan, J. Phys. Chem. B 107 (2003) 10967–10970.
[6] S. Orimo, Y. Nakamori, G. Kitahara, K. Miwa, N. Ohba, T. Noritakei, S. Towata, Appl. Phys. A 79 (2004) 1765–1767.
[7] W. Luo, J. Alloys Compd. 381 (2004) 284–287.
[8] Z. Xiong, G. Wu, J. Hu, P. Chen, Adv. Mater. 16 (17) (2004) 1522.
[9] H. Leng, T. Ichikawa, S. Hino, N. Hanada, J. Phys. Chem. B 108 (2004) 8763–8765.
[10] Z. Xiong, J. Hu, G. Wu, P. Chen, W. Luo, K. Gross, J. Wang, J. Alloys Compd. 398 (2005) 235–239.
[11] Y. Nakamori, S. Orimo, J. J. Phys. Chem. 370 (2004) 271–275.
[12] S. Hino, T. Ichikawa, N. Ogita, M. Udagawa, H. Fujii, Chem. Commun. (2005) 3038–3040.
[13] W. Luo, E. Ronnebro, J. Alloys Compd. 404–406 (2005) 392–395.
[14] W. Luo, S. Sickafoose, J. Alloys Compd. 407 (2006) 274–281.
[15] W. Luo, K. Stewart, J. Alloys Compd. 440 (2007) 357–361.
[16] http://www.draeger.com/ST/internet/US/en/Products/Detection/Drager-Tubes/ShortTermMeasurement/pd_shortterm_tubes.jsp.
[17] S. Luo, T.B. Flanagan, W. Luo, J. Alloys Compd. 440 (2007) L13–L17.
[18] Y.H. Hu, E. Ruckenstein, J. Phys. Chem. A 270–246 (2003) 9737–9739.
[19] E. Ruckenstein, Y. H. Hu, Patent number WO 2005/080266 A1, 2005.
[20] P. Hjort, A. Krozer, B. Kasemo, J. Alloys Compd. 237 (1996) 74–80.